



AIDA DART asteroid deflection test: Planetary defense and science objectives

Andrew F. Cheng^{a,*}, Andrew S. Rivkin^a, Patrick Michel^b, Justin Atchison^a, Olivier Barnouin^a, Lance Benner^c, Nancy L. Chabot^a, Carolyn Ernst^a, Eugene G. Fahnestock^c, Michael Kueppers^d, Petr Pravec^e, Emma Rainey^a, Derek C. Richardson^f, Angela M. Stickle^a, Cristina Thomas^g

^a JHU/APL, 11100 Johns Hopkins Rd, Laurel, MD 20723, USA

^b Université Côte d'Azur, Observatoire de la Côte d'Azur, CNRS, Laboratoire Lagrange, CS 34229, 06304 Nice Cedex 4, France

^c JPL, Pasadena, CA, USA

^d ESA/ESAC, Spain

^e Ondřejov Obs., Czech Republic

^f Univ. of Maryland, MD, USA

^g Planetary Science Inst, USA

ARTICLE INFO

Keywords:

Planetary defense
Asteroid impact hazards
Kinetic impactor
Binary asteroids
Hypervelocity cratering
Momentum transfer efficiency

ABSTRACT

The Asteroid Impact & Deflection Assessment (AIDA) mission is an international cooperation between NASA and ESA. NASA plans to provide the Double Asteroid Redirection Test (DART) mission which will perform a kinetic impactor experiment to demonstrate asteroid impact hazard mitigation. ESA proposes to provide the Hera mission which will rendezvous with the target to monitor the deflection, perform detailed characterizations, and measure the DART impact outcomes and momentum transfer efficiency. The primary goals of AIDA are (i) to demonstrate the kinetic impact technique on a potentially hazardous near-Earth asteroid and (ii) to measure and characterize the deflection caused by the impact. The AIDA target will be the binary asteroid (65803) Didymos, which is of spectral type Sq, with the deflection experiment to occur in October, 2022. The DART impact on the secondary member of the binary at ~6 km/s changes the orbital speed and the binary orbit period, which can be measured by Earth-based observatories with telescope apertures as small as 1 m. The DART impact will in addition alter the orbital and rotational states of the Didymos binary, leading to excitation of eccentricity and libration that, if measured by Hera, can constrain internal structure of the target asteroid. Measurements of the DART crater diameter and morphology can constrain target properties like cohesion and porosity based on numerical simulations of the DART impact.

1. Introduction

The NASA Planetary Defense Coordination Office (PDCO) was established in 2016 to address and plan response to the asteroid impact hazard. The mission of the PDCO is to detect any potential for significant impact onto Earth by natural objects and to develop strategies for mitigation of impact effects on human welfare. Under the auspices of the PDCO, the NASA Double Asteroid Redirection Test (DART) mission will demonstrate the deflection of a hazardous asteroid by a kinetic impactor. NASA will provide the DART mission element to the Asteroid Impact & Deflection Assessment (AIDA) mission, which is an international cooperation between NASA and ESA. The ESA mission element of AIDA will

be a rendezvous mission to characterize the target and measure the deflection outcome. The AIDA mission is similar to the ESA Don Quijote mission concept (Carnelli et al., 2006) studied in 2002–2007 but not funded for flight. The Don Quijote mission was designed to use a kinetic impactor to deflect an asteroid, changing its heliocentric orbit, and to observe this change with an additional rendezvous spacecraft, which would also characterize the target and study its physical changes after the impact.

Unlike Don Quijote, the AIDA mission (Cheng et al., 2015, 2016; Michel et al., 2016, 2017) is an international collaboration where NASA will provide the DART kinetic impactor. Also in contrast with Don Quijote, the target of the DART kinetic impact will be the secondary member

* Corresponding author.

E-mail address: andrew.cheng@jhuapl.edu (A.F. Cheng).

of the binary asteroid [65803] Didymos, which is a Potentially Hazardous Asteroid with minimum orbital intersection distance of 0.04 AU and $H = 18.1$. The objectives of the DART kinetic impact will be to change the binary orbit of this system, rather than the heliocentric orbit, and to observe the change.

The DART kinetic impact will be targeted to occur in October 2022 during a close approach of Didymos to Earth. The DART impact on the Didymos secondary (Didymos B) at ~ 6 km/s will alter the binary orbit period. The orbit period change can be measured by Earth-based observatories to confirm and quantify the amount of the deflection. Didymos is an eclipsing binary, which enables accurate determination of small period changes by ground-based optical light curve measurements (Pravec et al., 2006). In an eclipsing binary, the two objects pass in front of each other (occultations), or one object creates solar eclipses seen by the other, so there are sharp features in the lightcurves that can be timed accurately.

For the ESA mission element of AIDA, a Phase A/B1 study of the Asteroid Impact Mission (AIM) was completed in 2016. AIM was a mission to rendezvous with Didymos prior to the DART impact (Michel et al., 2016). However, AIM did not receive funding approval in 2016. ESA has continued study of a redesigned Didymos rendezvous mission, which is now renamed Hera. Launch of the Hera mission cannot occur before 2023, due to programmatic constraints on the European side, and Hera is planned to rendezvous with Didymos a few years after the DART impact. Hera is planned to characterize the target, to monitor results of the DART impact *in situ*, and to measure precisely the deflection resulting from the kinetic impact experiment.

The NASA and ESA mission elements of AIDA are independent but mutually supporting. The DART mission was approved for funding and entered NASA Phase B in June, 2017, with the Preliminary Design Review scheduled for April, 2018. This paper will focus on the DART mission. The Hera mission will begin an ESA Phase B1 study in early 2018 and will come before the ESA Council at Ministerial Level in late 2019 for funding approval. A detailed description of the Hera mission is given by Michel et al. (2017).

2. Aida mission rationale

AIDA will return fundamental new information on the mechanical response and impact cratering process at real asteroid scales, and consequently on the collisional evolution of asteroids, with implications for planetary defense, human spaceflight, and near-Earth object science and resource utilization. AIDA, with DART and Hera, will return unique and important information on an asteroid's strength, surface physical properties, and internal structure. Supporting Earth-based optical and radar observations, numerical simulation studies, and laboratory experiments will be an integral part of the AIDA mission.

2.1. DART objectives

Four primary strategies are identified as sufficiently mature to warrant consideration as approaches to mitigation of an asteroid impact threat (US NRC, 2010): civil defense warning, sheltering, and evacuating populations; impulsive deflection by a stand-off nuclear explosion; gradual orbit change with a nearby massive spacecraft (the “gravity tractor” concept); and impulsive deflection via addition of momentum by a kinetic impactor. Testing or demonstrating the nuclear detonation strategy in outer space is politically difficult and prohibited by international treaty.

DART will answer key questions about the kinetic impactor technique. As the first demonstration of asteroid deflection by a kinetic impactor, DART will provide important validation of the technique before it is considered viable for implementation in the event of an impact emergency. It will reduce risks and provide confidence for operations and decision makers. Kinetic impactors are useful (US NRC, 2010) in situations where an asteroid impact threat of up to hundreds of meters

diameter is identified years to decades before the Earth impact date. This warning time is sufficient for the kinetic impactor deflection to cause the asteroid to miss the Earth.

DART's kinetic impactor demonstration, targeted to Didymos B, will be conducted at a realistic scale for planetary defense. The target body, at a diameter of ~ 160 m, is large enough to be a Potentially Hazardous Asteroid (PHA) in its own right if it were a single body. If an NEO of this size were to impact Earth, it would release an impact energy of ~ 400 MT TNT and would cause regional devastation (over more than a metropolitan area). There are an estimated ~ 6700 PHAs at diameter ~ 140 m or larger (Harris and D'Abramo, 2015), most of which have not yet been discovered.

DART as part of the AIDA mission will also answer a key question about the kinetic impactor technique, which is that the magnitude of the resulting deflection is highly uncertain, owing to the poorly understood contribution of recoil momentum from impact ejecta. The impact ejecta carry off momentum back in the incident direction, so that the momentum transferred to the target can exceed the incident momentum by a factor that may be as much as 3 to 5 (Cheng et al., 2016; Holsapple and Housen, 2012; Jutzi and Michel, 2014; Stickle et al., 2015, 2017). The amount of momentum transferred from a kinetic impactor to an asteroid needs to be extrapolated from the centimeter scale of laboratory experiments by many orders of magnitude using models and numerical simulations.

DART will be the first high-speed impact experiment at an asteroid and at a realistic scale for planetary defense, where the impact conditions and the physical properties of the projectile are fully known, and furthermore with the Hera spacecraft the physical properties of the target will be characterized and the impact outcomes will be measured in detail. The efficiency of the momentum transfer strongly depends on the physical properties and internal structure of the target, notably density, porosity and strength (Cheng et al., 2016; Holsapple and Housen, 2012; Jutzi and Michel, 2014; Michel, 2013). No direct measurement of strength properties has been performed on any asteroid. Finally DART will determine, from terminal approach imaging, the impact location on the target asteroid, the local surface topography and the geologic context. Hera will further measure the size and depth of the crater made by the DART impact.

Key goals and measurements of the DART mission as the kinetic impactor element of AIDA are summarized in Table 1.

2.2. Hera rationale and objectives

Hera is a small mission whose objectives are to investigate the binary asteroid Didymos, to observe the outcome of a kinetic impactor test and thus, to provide extremely valuable information for mitigation, mining and science purposes (Michel et al., 2016, 2017). As the ESA part of the AIDA mission, Hera will rendezvous with the Didymos binary after the

Table 1
AIDA goals and measurements.

	Goals	Measurements
DART	Demonstrate kinetic impactor deflection of an asteroid by impacting Didymos B	Period change of the Didymos binary system induced by DART impact, with Earth-based observations
	Characterize the amount of deflection	
Hera	Improve modelling and assess momentum transfer efficiency of hypervelocity asteroid impact	Location of the impact site and local surface geology Sizes and shapes of Didymos A and B
	Assess momentum transfer efficiency of hypervelocity asteroid impact	
Hera	Determine asteroid density, porosity, and DART's crater properties to improve modelling estimates of asteroid impact effects	Mass of Didymos B Didymos orbital and rotational states Mass, shape and size of Didymos B DART crater size/morphology Surface disturbances and displacements induced by impact

impact on Didymos by the NASA DART mission (Cheng et al., 2016). It will make detailed measurements of the orbital and rotational states of the binary system, determine the physical properties of the target body Didymos B, particularly the mass, and investigate the impact crater from the DART impact.

Although DART will perform the impact on Didymos B in October, 2022 (Cheng et al., 2016), the planned launch of Hera, if approved, will be in October, 2023. Hera will arrive at Didymos in February, 2026, about 3.4 years after the DART impact. Important planetary defense objectives, such as measurement of the target mass to determine momentum transfer and DART crater morphology to constrain target physical properties, can still be met by Hera. There is no significant evolution of binary dynamics or crater morphology on a timescale of a few years.

Goals and measurements of the Hera mission as part of AIDA are summarized in Table 1, which shows that Hera will determine the momentum transfer by the hyper-velocity projectile DART and the outcome of its impact on Didymos B. In addition, Hera will carry, deploy and make the first use of a CubeSat in interplanetary space for spectral characterization of a small body. Hera will perform close-proximity operations in the environment of a binary system containing the smallest asteroid ever visited (Didymos B, 163 ± 18 m in diameter; Michel et al., 2016).

The Hera payload (see Table 2) will consist of two instruments and a CubeSat: the Asteroid Framing Camera (AFC), a laser altimeter (LIDAR) and a 6U CubeSat with two additional instruments: a hyperspectral imager called ASPECT (Asteroid SPECTral Imaging) and a second instrument which will be selected from among the following options: radio science, seismology, gravimetry or volatile detection. HERA will include a Radio Science Experiment (RSE), using the spacecraft telecommunications system. Optional payloads are under consideration, including a small carry-on impactor (SCI), which is a replica of the impactor carried by the Hayabusa-2 mission, and a high frequency radar sounder (HFR) for the measurement of subsurface properties. The Hera spacecraft design allows 40 kg mass for optional payloads.

The Hera measurements and measurement requirements, with associated payload instruments, are summarized in Table 2. Additional details on Hera payloads, requirements and objectives are given by Michel et al. (2017). Hera investigations of Didymos B's surface/internal properties and outcomes of the DART impact are of high value to address fundamental science questions and to support the planning of potential future asteroid mitigation, mining or sampling activities.

The Asteroid Framing Camera (AFC) is a flight spare of the NASA DAWN mission camera (Sierks et al., 2011a). The AFC is a 150 mm focal length, $f/7.5$ camera with $5.5^\circ \times 5.5^\circ$ FOV and $93.7 \mu\text{m}$ IFOV. The AFC will be used to study binary asteroid dynamics and physical characteristics including the mass of Didymos B, which is required to determine the momentum transfer from the DART impact. This will be obtained indirectly by measuring the reflex motion of the Didymos primary as it is orbited by the secondary. The mass of the primary is about 100 times the mass of the secondary, and thus the expected reflex motion radius is about one percent of the semi-major axis 1180 m, or about 10 m (Grieger

and Kueppers, 2016).

The LIDAR will determine the volume and shape of Didymos B by laser altimetry. The range accuracy is equal to or better than 50 cm, with a precision better than or equal to 20 cm. The sampling of the surface between footprints shall be 1 m or less by a footprint no bigger than 1 m in diameter, assuming pointing knowledge of 0.5 mrad (1-sigma) or better and a distance from the spacecraft to the surface of 10 km.

ASPECT (Kohout et al., 2017) will be carried by a 6U CubeSat that will be deployed by Hera in the vicinity of Didymos for imaging the surface of Didymos B at 2 m resolution and for obtaining chemical and mineralogical characterization of both binary components at spectral resolution <45 nm. ASPECT observes in the visible and near-infrared. It is a spectral imager from $0.5 \mu\text{m}$ to $1.6 \mu\text{m}$ and a point spectrometer from $1.6 \mu\text{m}$ to $2.5 \mu\text{m}$. The CubeSat will orbit Didymos at a distance of about 4 km.

The radio science experiment (Zannoni et al., 2017) will measure masses and gravity fields of Didymos A and B. After 8 close flybys for gravity science, the masses of the primary and secondary can be estimated to about 0.2% and 1.6%, respectively; the orbit of the secondary around the primary can be estimated to about 1 m; the pole orientation of the primary and the secondary can be estimated to about 0.1 deg and 0.4 deg, respectively (Zannoni et al., 2017).

Two optional payloads are considered for Hera, a monostatic high frequency radar (HFR) for sounding the Didymos B sub-surface and interior to a depth up to 10 m (Herique et al., 2017), and a Small Carry-On Impactor (SCI) offered by JAXA (Saiki et al., 2017). SCI is to perform an impact experiment on Didymos B, using an explosively formed, 2 kg copper projectile at ~ 2 km/s.

3. Dart mission and spacecraft

The DART mission will impact the secondary member of the Didymos binary system during its close approach to Earth in October, 2022. The impact of the ~ 525 kg DART spacecraft at 6 km/s will produce a binary orbit period change of ~ 7 min, assuming that the incident momentum from the impactor is simply transferred to the target without enhancement (Cheng et al., 2016). This change in binary orbit period can be measured within a week of observing with telescopes of aperture as small as 1 m. Thus the occurrence of the target asteroid deflection is confirmed, and the amount of the deflection is quantified, by ground-based observations to measure the binary orbit period change.

The DART target is the secondary component of the binary system (65803) Didymos. This satellite orbits its primary with a period of 11.9 h, a semi-major axis of 1.1 km, and a nearly circular orbit (Pravec et al., 2006). The primary has a diameter of 780 m, the secondary 160 m. The presence of a satellite has allowed the density of the primary to be estimated as 2.1 g/cm^3 (Michel et al., 2016). Ground-based reflectance spectroscopy of Didymos (Dunn et al., 2013) shows it to have ordinary chondrite-like spectral parameters, so it is a member of the S-complex, the most common compositional group of near-Earth objects.

The DART kinetic impactor spacecraft baseline design has changed

Table 2
Hera required measurements and instruments.

Parameter	Measurements	Payload instruments
Size, mass, shape, density	Mass: 10% Density: 20%	mass from binary orbit, spacecraft tracking (AFC, ASPECT, RSE)
Dynamical state: period, orbital pole, spin rate, spin axis	Global shape: <5 m lateral resolution and 2 m height resolution Orbital period already known to $<0.1\%$ Orbital pole: 5° Spin rate: 1% Spin axis: 1°	shape model (AFC, LIDAR) AFC
Physical properties, topography, DART impact crater properties	Global surface resolution: 1 m Local surface resolution (10% of surface): 10 cm	AFC (surface features), ASPECT (2 m-resolution)
Mineral composition of Didymos A and B	Spectral resolution: 40 nm for all color filters except AFC near-IR (980 nm) with 80 nm width	ASPECT, AFC

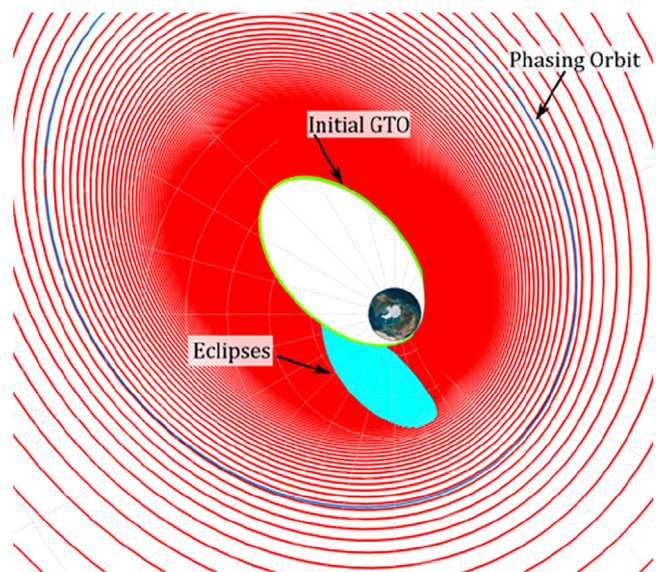


Fig. 1. DART departs Earth using a low-thrust spiral over 7–9 months. The engine shuts off for eclipses (cyan) and phasing arcs (blue). (For interpretation of the references to color in this figure legend, the reader is referred to the Web version of this article.)

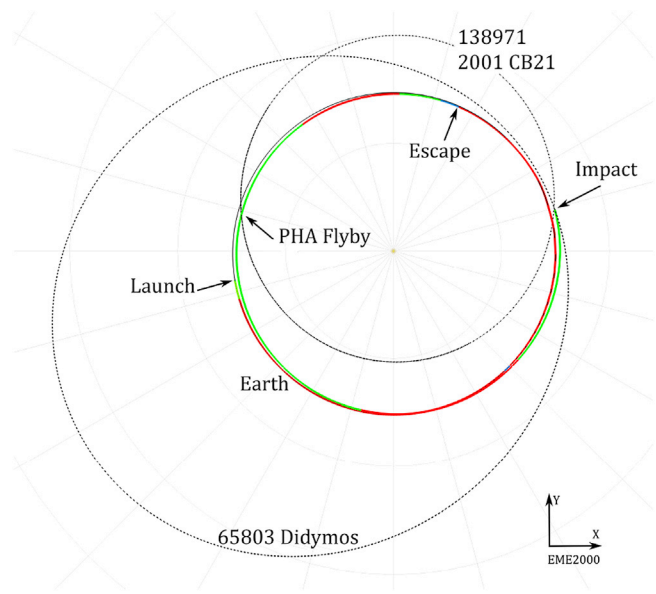


Fig. 2. DART remains in a near-circular orbit at 1 AU, using low-thrust to drift ahead of Earth and achieve an out-of-ecliptic component to impact Didymos at conjunction. Red, thrust arcs; green, coast arcs. (For interpretation of the references to color in this figure legend, the reader is referred to the Web version of this article.)

from that described by Cheng et al. (2016). The DART spacecraft will use an ion propulsion system, the NASA Evolutionary Xenon Thruster (NEXT). DART is currently designed to be launched as a secondary payload on an Evolved Expendable Launch Vehicle to geosynchronous transfer orbit (GTO). DART will use the NEXT system to spiral out from Earth orbit (see Fig. 1) and to thrust to Didymos on an interplanetary trajectory, with encounter at Didymos in October, 2022 (see Fig. 2). The Didymos encounter for the ion propulsion mission occurs in the same time frame and a similar geometry as for the chemical mission design (Cheng et al., 2015, 2016).

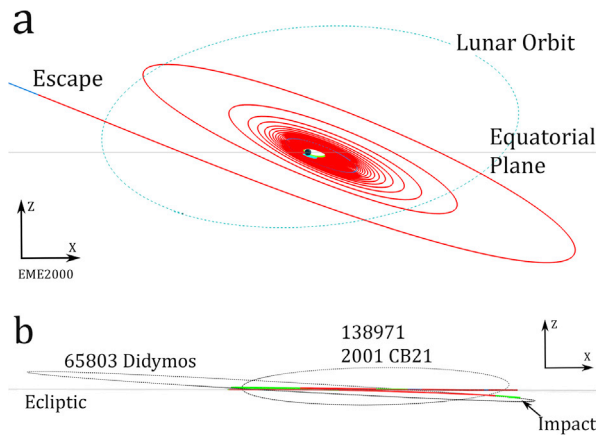


Fig. 3. Panel a. DART is launched into an inclined orbit, avoiding the Moon and escaping in a favorable direction for the 2001 CB21 flyby. Panel b. The Didymos impact occurs south of the ecliptic near perihelion.

Table 3
DART reference mission design.

Launch Date	Mar. 31, 2021
Earth Escape Date	Dec. 05, 2021
2001 CB21 Flyby Date	Mar. 06, 2022
2001 CB21 Flyby Speed	11.47 km/s
Didymos Impact Date	Oct. 05, 2022
Didymos Arrival Speed	5.966 km/s
Time of Flight	553 days
Maximum Earth Distance	0.08 AU
Solar Distance	0.97 AU–1.03 AU
Earth Distance at Impact	0.07 AU
Solar Phase Angle	60°
Impact Angle to Orbit Plane	15.7°

DART is designed to be able to launch to GTO on any day from December 15, 2020 through March 31, 2021. For most of the Earth spiral orbit phase (see Fig. 3), DART points NEXT along the Earth-relative velocity to increase its altitude. Earth escape occurs on Dec. 5, 2021, with DART targeted to a flyby of the PHA [138971] 2001 CB21 on Mar. 6, 2022. NEXT thrusting arcs are planned for the interplanetary trajectory to impact the Didymos secondary on Oct. 5, 2022. The DART reference mission design is summarized in Table 3.

The DART trajectory remains near 1 AU from the Sun and has a maximum Earth distance of 0.08 AU. The impact speed on Didymos is 5.966 km/s, and the approach direction is at an angle of 15.7° to the orbital plane of Didymos. The approach solar phase angle at 60° is favorable for imaging of target surface features.

Fig. 4 shows the DART spacecraft in its stowed and deployed configurations. The DART payload consists of a single instrument, the visible imager DRACO (Didymos Reconnaissance and Asteroid Camera for OpNav).

4. DART imaging

DART carries the narrow angle visible imager DRACO to support the primary mission objectives of impacting the target body through its center and characterizing the impact site. DRACO is required to support optical navigation on approach and autonomous navigation in the terminal phase. DRACO is derived from the New Horizons LORRI instrument (Cheng et al., 2008) and will use a 20.8 cm aperture, f/12.6 Ritchey-Chretien telescope to obtain images at 0.5 arc sec per pixel, with a 0.29° × 0.29° field-of-view. DRACO is a panchromatic imager and uses the BAE CIS2521 5.5 Megapixel CMOS image sensor.

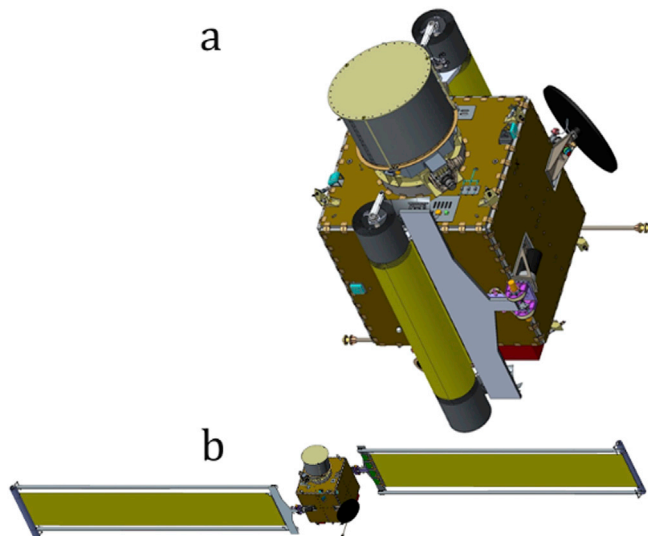


Fig. 4. DART in its stowed (a) and deployed (b) configurations. In both configurations the gimbaled NEXT thruster is at top and the DRACO imager is at bottom (hidden). Dimensions of the spacecraft box are $1.14 \text{ m} \times 1.24 \text{ m} \times 1.32 \text{ m}$, where the edge closest to the viewer in panel (a) is 1.24 m . The edge closest to viewer in panel (b) is 1.14 m . DART has 22 m^2 roll-out solar arrays, 12 hydrazine thrusters, a radial-line-slot array high-gain antenna, two low-gain antennas, a star tracker, and 5 Sun sensors.

The DART observation timeline at Didymos can be split into three phases:

- a) **Long-range phase:** The long-range phase begins when the Didymos system is first acquired by DRACO, ~ 30 days before impact, and extends until the terminal phase begins. During this phase, DRACO acquires a long-range suite of observations where the Didymos system is mostly not resolvable. Light curve information complementary to ground-based observations will be extracted from these images.
- b) **Terminal phase:** The terminal phase begins with the initiation of DART's autonomous navigation, ~ 4 h prior to impact, and extends until the final phase begins. During this phase, the separation between Didymos A and B can be resolved, and DRACO images support both autonomous navigation and characterization of Didymos A and B.
- c) **Final phase:** The final phase comprises the last ~ 2 min of the DART mission. During this phase, all DRACO images will be devoted to characterization of Didymos B, as autonomous navigation will have been completed. At ~ 17 s prior to impact, DRACO achieves its requirement to image Didymos B at a pixel scale of ≤ 50 cm (with 2×2 binned pixels). Higher-resolution images will continue to be acquired in the final seconds of the mission. Planned real-time DSN coverage enables downlink of these images to Earth, including all images acquired 5 s before impact (down to ~ 15 cm 2×2 binned pixel scale) and earlier, and possibly including images acquired during the final 5 s.

The imaging data collected by DRACO will address three main objectives of the DART investigation team: (1) to refine pre-encounter estimates of the Didymos A rotation rate and Didymos B orbit and search for additional system members; (2) to characterize the global shape and surface geology of Didymos A and B; and (3) to characterize the local surface properties and slope of the DART impact site on Didymos B. These objectives are described in more detail below. The DRACO observation sequence will also be exercised during the flyby of 2001 CB21, seven months before the Didymos encounter (see Table 3).

4.1. Observe Didymos a rotation rate and didymos B orbit; search for additional bodies

DRACO collects long-range images on approach, before the Didymos system is resolvable. These images are needed for optical navigation to the system, and together will be used to obtain light curve information at viewing geometries complementary to those obtainable by ground-based telescopes. Using approaches employed by previous studies (Pravec et al., 2006; Viikinkoski et al., 2015; Weaver et al., 2016), these lightcurves will tighten constraints on the rotation rate and shape of Didymos A, and the orbital period and shape of Didymos B. In addition, these long-range images will be used to search for any additional satellites.

4.2. Characterize the global shape and surface geology of Didymos A and B

In the current imaging plan, about 45 min before the DART impact, Didymos B becomes a resolved object in DRACO images. Images containing both Didymos A and B are planned to continue until ~ 4 min prior to impact, when the 2×2 binned pixel scale is 7 m. After this time, portions of Didymos A will extend beyond the DRACO field of view as the DART spacecraft continues to advance toward Didymos B. The final planned images containing small portions of Didymos A will be acquired ~ 2 min prior to impact, with a pixel scale of 3.5 m.

Shape models of Didymos A and B will be produced from the images using stereophotoclinometry (SPC) (Gaskell et al., 2008). SPC combines traditional stereo techniques with photoclinometry to estimate the heights across small patches of the surface (called maplets) from multiple images acquired during approach. The impact trajectory limits stereo information for the high-resolution images, but limbs will be incorporated to constrain maplet positions. The DART team will further constrain the shapes of both Didymos A and B, in particular the portions not observed by DRACO in high-resolution images, by incorporating light curve data collected both during the long-range phase and by ground-based observations. The shape modeling effort will also take advantage of changes in surface illumination observed as Didymos A rotates and Didymos B orbits for the ~ 1 h of resolved imaging when the pixel scale is too large to contribute to maplets topography. SPC has been successfully used to construct shape models from small body flybys (e.g., Steins, Lutetia, Phoebe), and Sierks et al. (2011b) demonstrate that for Lutetia, the combination of constraints on rotation axis, ground-based lightcurves, and an SPC-derived shape model produced a derived volume with less than 10% error.

Resolved images that contain both Didymos A and B will allow characterization of the shapes and large-scale geological properties of both bodies, and will be sufficient to map and measure features such as craters and large blocks, and to assess the distribution of smooth versus rough terrain and albedo variations. The images will enable comparisons between the two bodies, which will be important to interpret the origin and evolution of the binary system. In addition, the images will allow comparisons to similarly sized asteroids that have been (or will have been) visited by spacecraft: Itokawa (visited by Hayabusa); Ryugu and Bennu (the targets of Hayabusa2 and OSIRIS-REx, respectively). The radar shape model of Didymos A is similar to the top-like shapes of Bennu and the 1999 KW4 (66391) primary. These shapes may result from a common spin-up mechanism driven by thermal YORP (Walsh et al., 2008; Jacobson and Scheeres, 2011) which may lead to binary formation.

The surface of Itokawa was revealed to have few craters, but numerous blocks (Fujiwara et al., 2006). In this case, the size-frequency distribution of craters provides a broad range of possible surface ages (Michel et al., 2009). On very small objects like Didymos A and B, blocks are likely to be more numerous than craters, and may serve as better tools to assess the surface processes on these asteroids. Assessments of block shapes (e.g., Michikami et al., 2010, 2016; Noguchi et al., 2010; Marshall and Rizk, 2015) and size-frequency distributions (e.g., Michikami et al., 2008; Mazrouei et al., 2014; Noviello et al., 2014; Tancredi et al., 2015)

have been used to gain new insights on the processes that have led to the current surface state of Itokawa. Itokawa's blocks provide evidence for the rubble-pile nature of the asteroid (Fujiwara et al., 2006). Blocks and regolith as found on Itokawa could not have formed on a body the size of Itokawa and suggest that Itokawa formed after a catastrophic disruption event (Cheng et al., 2009).

The distribution of rough versus smooth terrain on Itokawa is highly correlated to gravitational potential; fine regolith is thought to have flowed “downhill” from what are now the rough highlands to the smooth lowlands (e.g., Fujiwara et al., 2006; Saito et al., 2006; Miyamoto et al., 2007; Barnouin-Jha et al., 2008). The distribution of regolith (from large blocks to cobbles to fines) and albedo patterns on Didymos A will provide insights into the motion of material on the surface and formation of the Didymos binary system. If the system was formed by YORP spinup, evidence of mass movement towards the equatorial regions may be apparent (Walsh et al., 2008). If mass shed from these regions contributed to or formed Didymos B, the satellite may look like a rubble pile and should have spectral similarities to Didymos A.

4.3. Characterize the local surface properties and slope of the DART impact site on Didymos B

The DRACO images acquired during the final minutes of the DART mission provide high-resolution views of Didymos B and the DART impact site. DRACO is required to image Didymos B at a pixel scale of ≤ 50 cm, to determine the location and surface characteristics of the DART impact site. Experience from prior asteroid missions such as NEAR-Shoemaker and Hayabusa have shown that images at this pixel scale (e.g., Fig. 5) are more than sufficient to characterize the target surface and resolve features at the scale of the DART spacecraft (Fig. 4), including surface roughness, blocks, craters, and lineaments.

The highest-resolution images will be used to characterize the impact site and surroundings in more detail than the body as a whole. Observations of surface roughness will be made, distinguishing between areas covered in cobbles or sand-sized regolith grains versus those with a more blocky appearance. Higher-resolution images will allow the measurement of the block and crater populations that are complete down to sizes



Fig. 5. Hayabusa image of Itokawa at 50-cm pixel scale. Planned DRACO imaging will achieve the required 50-cm pixel scale ~ 17 s prior to impact, and higher resolution images will continue to be acquired and downlinked during the final seconds of the mission.

~ 5 times the image pixel scale. Assessments of roughness and surface structures, particularly blocks, will be key for assessing the initial impact conditions. If the impact occurs into terrain covered in blocks at the scale of the spacecraft, the coupling of the spacecraft to the target will be different and lead to a different momentum transfer than if the impact occurs onto relatively smooth regolith.

The images, in conjunction with the shape model, will be of sufficient resolution to estimate the regional surface slope at the impact site. The precision of regional slope estimates is dependent on the local phase angles of the images. The slope estimate from DRACO imaging is expected to be better than 10° for the current 60° phase angle images that are planned. Testing with simulated images will provide a better estimate of the precision to which surface tilt can be measured. The images will also be critical for mapping the extent of loose regolith and to establish any relationship to regional slope and local geopotential altitude (Scheeres et al., 2016).

The local surface properties and slope of the impact site, in addition to the internal structure of the asteroid, will influence the momentum transfer that occurs during the DART impact. It is therefore important to assess these factors with DRACO in order to understand the implications of the observed beta values from the impact, to inform numerical simulations of the event, and to gauge the generic effectiveness of a kinetic impactor for hazard mitigation.

4.4. Exercise DRACO observation sequence during an asteroid flyby

The mission design for DART includes a flyby of the near-Earth asteroid 2001 CB21 in March, 2022 for any launch date within a three-month window from December 2020 to March 2021. The asteroid flyby allows a dress rehearsal for most of the Didymos encounter activities except for the impact. A performance analysis of the autonomous targeting algorithm will be obtained during the flyby encounter, during which the autonomous navigation will be active but will not be able to alter the spacecraft trajectory. The flyby target also serves as a calibration target for DRACO to allow its performance to be better characterized. The acquired images will be used to characterize the target's shape and surface properties.

5. Observation campaign strategy

An observing campaign in support of the DART impact is a critical piece in obtaining the data necessary for mission success. The DART project will follow in the footsteps of several earlier efforts, such as those for the Shoemaker-Levy 9 impact, Comet ISON's apparition, and the LCROSS and Deep Impact missions (among others), in coordinating astronomers around the world to observe prior to, during, and after the impact period.

Didymos has been extensively observed from the ground during its 2003–2004 close approach to Earth at 0.05 AU, and the basic properties of the Didymos system as currently understood are mostly derived from optical observations and radar measurements made during that

Table 4
Didymos apparitions.

Opposition Date	Peak V Mag ^a	Solar Elong.	Min. Earth Dist. (AU)
10 Apr 2015	20.58	175°	1.24
27 Mar 2017	20.35	174°	1.14
13 Mar 2019	19.89	173°	0.97
20 Feb 2021	19.01	172°	0.70
19 Aug 2022	14.54	124°	0.07
10 Jan 2023	16.58 ^b	171°	0.30 ^b

^a The peak V magnitude does not always occur on the opposition date. Solar elongation is at peak brightness.

^b Over 2022–2023 Didymos retreats from Earth and has two distinct opposition times. The V magnitude and Earth distance for 2023 are listed for the opposition date.

apparition (Pravec et al., 2006; Scheirich and Pravec, 2009; De Leon et al., 2010; Benner et al., 2010).

Additional observations will reduce mission risk and improve interpretations of impact results. Because Didymos is faint ($V > 18.9$) and distant (>0.7 AU) until the 2022 apparition, and given the current state of knowledge, only a few techniques are appropriate for observations in the apparitions prior to 2022. Spectroscopy is possible, but high-quality time-resolved observations during mutual events will be difficult or impossible during pre-2022 observations. Didymos is too distant for radar observations prior to 2022. Table 4 shows the optical observing windows between 2015 and 2023.

5.1. Observations during the impact apparition

The DART mission requires measuring the Didymos binary period change from the DART impact to a precision of 7.3 s. This requirement is reachable with current equipment, modest apertures as small as 1 m, and well-established techniques. For instance, Polishook et al. (2011) report an orbit period of 33.385 h for a satellite of (3749) Balam with an observational uncertainty of 3.6 s. These observations were made with a 1-m and a 0.46-m telescope with 11 nights of observing over the course of 5 months when Balam's R magnitude <17.5 . Given the availability of a larger number of much larger telescopes, a comparable observational period post-impact with Didymos at $R < 17.5$, a much shorter orbital period to measure, and radar measurements, the 7-s requirement is readily achievable.

Table 5 shows a non-exhaustive list of observatories that can observe Didymos in the 2022 apparition. Nearly continuous coverage by large telescopes (4 m class or larger) can be obtained, save for a gap in longitudes between Australia and South Africa where only smaller telescopes exist (Fig. 6). Because Didymos B completes about two orbits per Earth day, every orbit phase is observable from at least one site with a large telescope every 24 h, with many of those orbit phases observable from more than one site.

During the 2022 apparition coinciding with the DART impact, Didymos will be a moderately strong radar target at Goldstone and an imaging target at Arecibo. The asteroid will approach from the south, enter Goldstone's declination window beginning on September 25, and enter Arecibo's observing window on October 24. Current mission design places the impact on 5 October, observable with Goldstone but not Arecibo. Using the newest pole estimate, the line-of-sight will be along the orbit plane in mid-November. If so, then eclipses and occultations will

Table 5
Optical and infrared observing facilities.

Facility	Telescopes	Location	Note
IRTF	1 × 3.0 m	Mauna Kea	1
Keck	2 × 10.0 m	Mauna Kea	1,2,3
Gemini	2 × 8.0 m	Mauna Kea	1,2,3,4,5
		Chile	
Magellan	2 × 6.5 m	Chile	1,2,4,5
Las Campanas	1 × 2.5 m	Chile	2,4
DCT	1 × 4.3 m	Arizona	1,2,4,5
WHT	1 × 4.2 m	Canary Islands	1,2,3,4,5
ESO	4 × 8.2 m, 1 × 3.6 m, 1 × 3.5 m	Chile	1,2,3,4,5
GTC	1 × 10.4 m	Canary Islands	2,4
MRO	1 × 2.4 m	New Mexico	2,4
LCOGT	11 × 1 m, 2 × 2 m	N Hemisph.* S Hemisph.**	2,4
IUCAA	1 × 2.0 m	India	4
AAO	1 × 3.9 m	Australia	1,5
SAAO	1 × 11.0 m, 1 × 1.9 m	South Africa	2,4

*1 × 2 m, 3 × 1 m **1 × 2 m, 8 × 1 m

Notes. 1. IR spectroscopy. 2. Optical spectroscopy. 3. Adaptive optics. 4. Optical imaging. 5. IR imaging.

be visible in radar images at Arecibo. If the orbital period of the secondary changes by at least 1% due to the impact, then the change in the position of the secondary should be evident in delay-Doppler radar images at Arecibo and possibly at Goldstone within roughly three weeks. The long time baseline of radar observations between Goldstone (pre-impact) and Arecibo (post-impact including after period of Goldstone visibility) suggests that orbital changes might be detectable by radar, independent of other measurements, if the pre-impact position is known very well.

If the DART impact generates ejecta with abundant centimeter- and decimeter-scale particles, then Arecibo (and possibly Goldstone) might detect a cloud in a manner similar to coma detections from comets. In Doppler-only echo power spectra of comets, coma echoes appear as a broad “skirt” surrounding the nucleus, which appears as a narrow spike in Doppler frequency. If the ejecta consist of much smaller-sized dust, as was the case with the Deep Impact mission at comet Tempel 1 (Holsapple and Housen, 2007), then the ejecta probably will not be detectable with radar.

6. Impact modeling

Planetary impact experiments are useful to scale the understanding from decades of laboratory-scale impact experiments to impacts on solar system bodies. For a solar-system impact, the projectile and the target properties, as well as impact angle and velocity, are unknown. In contrast, both the target and projectile materials and the impact parameters are known in laboratory experiments. Here, the projectile (the DART spacecraft) mass, material properties, impact angle and speed are known, but target properties are unknown. In order to fully understand the effectiveness of kinetic impact deflection, though, the target properties—and their effect on the impact process—must be understood. Some *a priori* estimates can be made to help plan observations prior to the impact, and various numerical and analytical models can probe possible outcomes. Despite these unknowns, planetary impact experiments are vital to understand the results of large-scale impacts, and the DART impact provides our first opportunity to test asteroid deflection at real asteroid scales and to test the accuracy of impact models for kinetic impactors.

Many variables affect the outcome of the DART impact onto Didymos B, including mechanical properties of the target body, such as strength, density, material composition, and porosity, as well as internal structure and shape of the body. Local topography and the presence of boulders at the impact site can affect the impact outcome. To better constrain these variables and to understand their effects on impact outcomes and momentum transfer efficiency, a large-scale impact modeling campaign is a part of the DART project. Impact modeling provides a basis for interpretation of DART impact observations (including the calculation of the momentum enhancement, β , the period change, and ejecta mass for a given impact scenario).

Currently there are two main activities as part of the modelling campaign for the DART mission. The first is a community-wide attempt to benchmark various hydrocodes against one another in the strength regime [e.g., Stickle et al., 2016]. The main impact hydrocodes were benchmarked against one another by Pierrazzo et al. (2008), and found to have a natural variation of 10–20%. However, these initial comparisons were done using strengthless targets. Because the gravity of Didymos B is low, the DART impact will be strength-controlled (Cheng et al., 2016), and target material strength will be important in the ejecta evolution and crater formation following impact. Several types of numerical methods can be used to model the DART impact, all of which differ in their fundamental approach to solving flow equations as well as modeling of material properties and responses to impact stresses. Initial comparisons of impact hydrocodes against one another when strength models are implemented show a variation of 10–15% ([Stickle et al., 2016]). This variation is likely due to the ways in which material models are implemented into the different hydrocodes, and understanding the

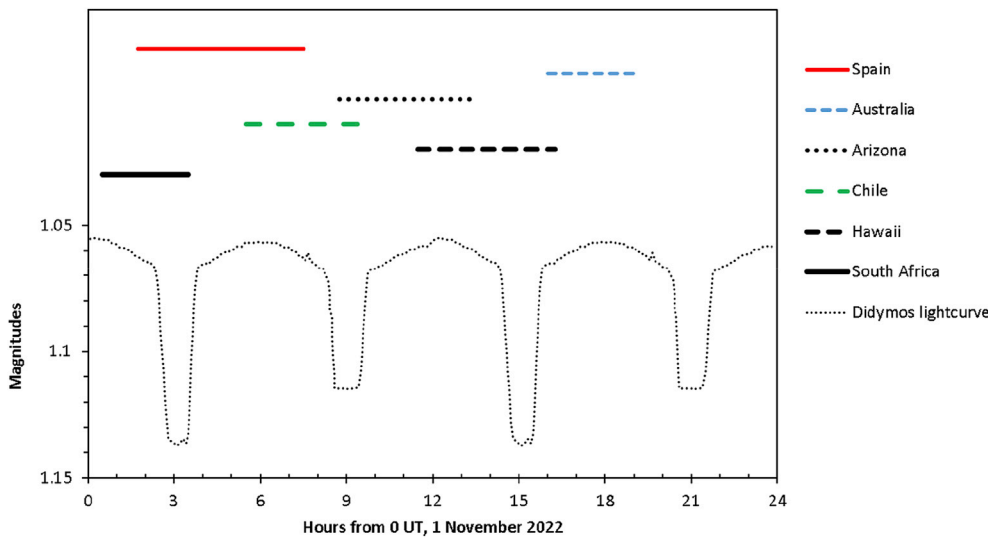


Fig. 6. The coverage available for Didymos over a 24-h period is schematically shown here for 1 November 2022. The time span for which Didymos is more than 30° above the horizon and the Sun is below the horizon is shown as a horizontal range for each of 6 different observing sites, offset from one another: the Canary Islands, Spain; the AAO in Siding Spring, Australia; Kitt Peak, Arizona; ESO in Chile; Mauna Kea; and Sutherland, South Africa. The bottom trace represents the light curve of the Didymos system (arbitrary magnitude offset), with the dips representing mutual events. The phase of the light curve relative to the x-axis is arbitrary. There is complete coverage, often with simultaneous observations possible, for nearly 20 h from when Didymos is high enough in the sky to observe in South Africa until sunrise in Australia.

magnitude of these differences allows us to compare large-scale simulations between different codes.

The second main activity is to better understand the range of possible outcomes of the DART impact when variations in target parameters are considered. This is done using large-scale impact models.

Simulations calculated the momentum enhancement factor β (the ratio of momentum transferred by impact to incident momentum) and studied its sensitivity to parameters such as impact angle, target microporosity, and location of impact (e.g., Stickle et al., 2015, 2017; Syal et al., 2016), finding a range of β values between ~ 1 and 5 and crater depths ranging from approximately 2–4 m and diameters of ~ 5 –14 m (Stickle et al., 2015). Preliminary calculations also suggest that local slope at the impact site can affect effective β values by 20% for otherwise identical impact conditions. Specifics of material composition appear to have little effect on the expected momentum transfer following the DART impact (e.g., Stickle et al., 2017). The calculations suggest that the yield strength of the material and porosity have the most important effects on crater morphology and β (Rainey et al., 2017; see Fig. 7).

Material porosity can come in the form of “microporosity” where

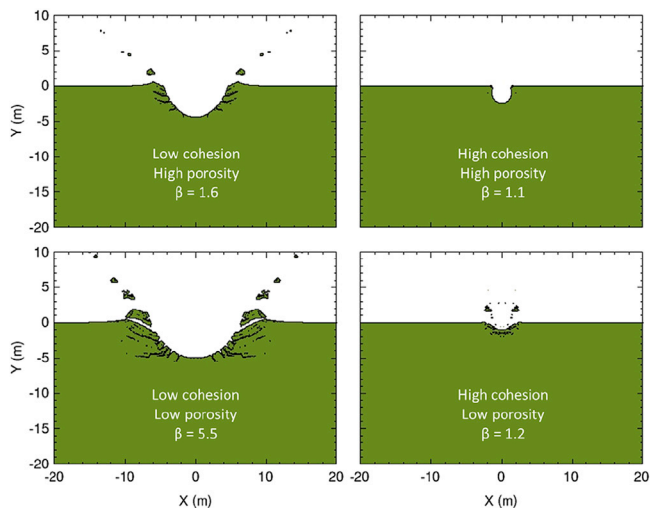


Fig. 7. Four material plots from 2D axisymmetric CTH simulations for high and low values of target cohesion (100 MPa and 0.1 MPa, respectively) as well as microporosity (40% and 0%, respectively). Impactor in all cases a 520 kg Al sphere at 6 km/s. These cases illustrate the potential to constrain target physical properties with post-impact measurements of β and crater morphology.

there is void space among grains in the material, or “macroporosity” where the void space is along large-scale cracks or between large boulders if the asteroid is a “rubble pile”. Both of these porosity types will affect the ejecta generated following impact (Fig. 8), and thus the eventual momentum enhancement from the kinetic impact. In general, as microporosity in the target increases, the crater becomes increasingly narrow and deep, and the shape of the subsurface damage zone is altered. The ejecta is launched at higher angles for increasingly high porosities.

When the target has an equivalent macroporosity instead of microporosity, the crater tends to be larger with an increased amount of ejecta. Some care must be taken when modeling macroporous targets, however. Depending on the structure of the target (e.g., amount, size, and location of large boulders), impact outcomes can vary significantly (Fig. 8). If the

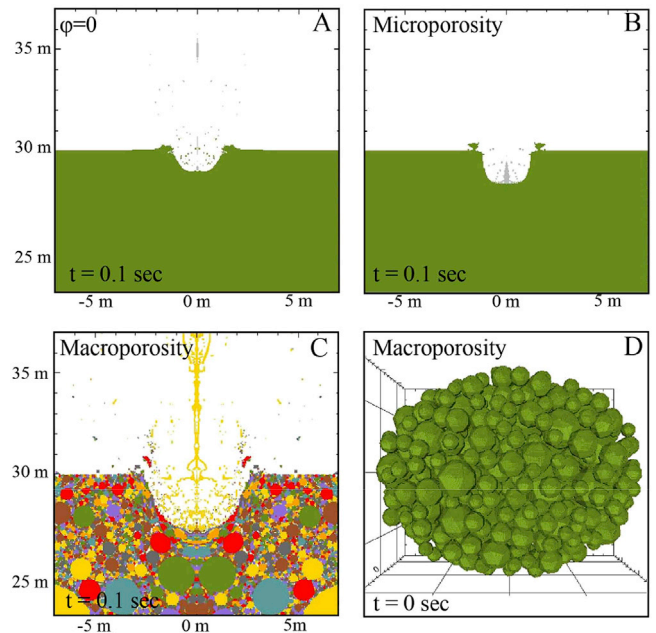


Fig. 8. CTH hydrocode models of impacts into targets with various material properties. 2D models of a 30-cm aluminum sphere at 6.25 km/s into A) coherent, basalt target with no porosity; B) coherent basalt target with 20% microporosity; C) rubble pile target with equivalent 20% macroporosity. The high ejecta plume in the center is a center-line effect in the 2D simulation; D) Example of a 3D rubble pile asteroid to model impacts into matrix with boulders and a variety of subsurface structures.

Table 6
Physical properties of (65803) Didymos.

Primary Diameter	0.780 ± 10% km
Secondary Diameter	0.163 ± 0.018 km
Total System Mass	(5.278 ± 0.54) × 10 ¹¹ kg
Component Bulk Density ^a	2100 km m ⁻³ ± 30%
Primary Rotation Period	2.2600 ± 0.0001 h
Component Separation	1.18 + 0.04/−0.02 km
Secondary Orbital Period	11.920 + 0.004/−0.006 h
Didymos Spectral Type	Sq

^a Assumed the same for primary and secondary.

spacecraft were to impact onto a large, strong boulder, for instance, the cratering process and ejecta flow field will be significantly different than if the spacecraft were to impact into weaker granular matrix between boulders. Initial simulations show that the momentum enhancement factor can depend on structural features of the impact site [Stickle et al., 2017; Owen et al., 2017]. Terminal imaging from DRACO will allow this to be better constrained following the DART-impact, and these processes are under further investigation.

7. Didymos binary system dynamics & physical properties

To fully interpret the outcomes of the DART impact, it is necessary to understand physical properties of the target body and the binary system dynamics, including natural perturbations of the orbit period. Table 6 gives some basic physical parameters of Didymos and its current dynamical and rotational states (Michel et al., 2016).

The secondary is assumed to orbit in the equatorial plane of the primary. Put another way, the primary spin pole and mutual orbit pole are assumed to be co-aligned, with negligible precession. Fig. 9 shows the current primary shape model derived from radar and light curve observations. The same observations do not support the derivation of a shape model for the secondary. The secondary is assumed to be in synchronous rotation with its orbit (averaging over any libration modes).

7.1. Spectral type

The visible-NIR spectrum of Didymos is ordinary chondrite-like based upon analyses of the 1 μm band center and the band area ratio 2 μm band/1 μm band (Dunn et al., 2013). Using the Didymos spectrum from

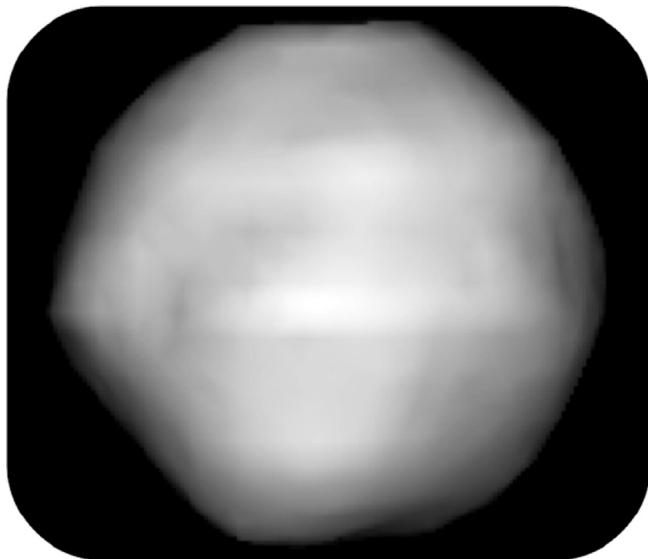


Fig. 9. Preliminary shape model of the primary from combined radar and light curve data, diameter ~780 m. The secondary (not imaged) is estimated to be more elongated.

De Leon et al. (2010), we determined additional spectral parameters defined by DeMeo et al. (2014): the 1 μm band minimum at $0.965 \pm 0.002 \mu\text{m}$, depth of 0.043 ± 0.01 , width $0.231 \mu\text{m}$ and area $0.0066 \mu\text{m} \pm 0.002 \mu\text{m}$; also the slope $-0.4 \pm 0.2 \mu\text{m}^{-1}$ on the short wavelength side of the minimum, and finally the potential depth 0.26 ± 0.1 relative to the reflectance at $1.5 \mu\text{m}$.

In the classification scheme of DeMeo et al. (2014), the types Q or Sq both have band minimum $>0.96 \mu\text{m}$ (true for Didymos). In addition, type Sq requires at least one of the following: slope $\geq -0.75 \mu\text{m}^{-1}$ (true), or band area $<0.016 \mu\text{m}$ (true), or potential depth <0.2 (not true, but within the error bar), or the condition [slope $> -1 \mu\text{m}^{-1}$ and depth <0.08] which is true. Didymos can be assigned unambiguously to spectral type Sq, consistent with the findings of Dunn et al. (2013).

7.2. Primary structure

The Didymos primary is close to if not beyond the spin rate limit for loose material to remain on the surface at the equator. Weak cohesion ($<100 \text{ Pa}$) may be implied, although there is sufficient uncertainty in the shape model and in the bulk density that zero cohesion cannot yet be ruled out. Based on the estimated bulk density, the primary is likely a gravitational aggregate or rubble pile. Modeling of the distribution of internal components is compatible with a mass distribution where the largest component is in the range 15%–50% of the whole mass (Campo Bagatin et al., 2018).

Fig. 10 shows the failure mode diagram of the primary (indicating the degree of cohesion needed to maintain its shape as a function of spin period), based on a continuum analysis (Hirabayashi and Scheeres, 2016) of the current best shape model, assuming uniform internal structure and the nominal bulk density. A Drucker-Prager model is used for the yield condition, and the friction angle is fixed at 35° . Two distinct failure modes are found, if there is insufficient cohesion/friction. If Didymos fails at a spin period longer than 3.0 h, only the equatorial region fails. Otherwise, the internal structure should fail first.

A soft-sphere discrete-element model (Schwartz et al., 2012) has been used (Zhang et al., 2017) to explore the conditions needed for a rubble-pile primary made up of self-gravitating spheres to hold its shape. Gravel-like material properties (friction angle 40°) with rolling friction included give a stable outcome without cohesion for bulk density $>2600 \text{ kg m}^{-3}$ when the spheres are packed randomly and compactly, and at lower densities for hexagonal-close-pack configurations.

Fig. 11 shows the shear stress distribution over a cross-section for a stable random-packed case. Analysis of this case shows that it is everywhere below the Mohr-Coulomb yield condition.

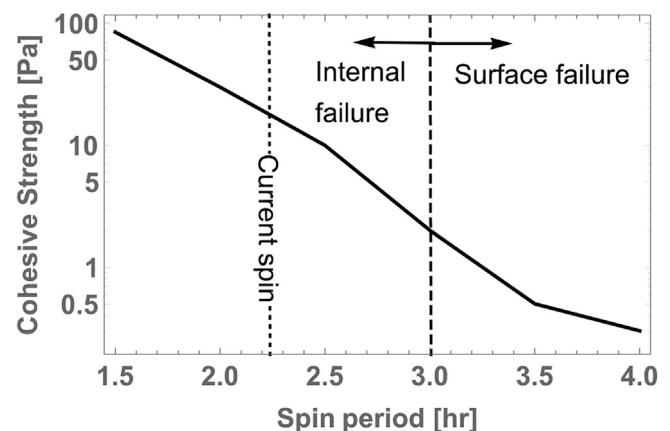


Fig. 10. Didymos failure mode plot. The current spin period is 2.26 h; the boundary between surface failure and internal failure is ~3 h.

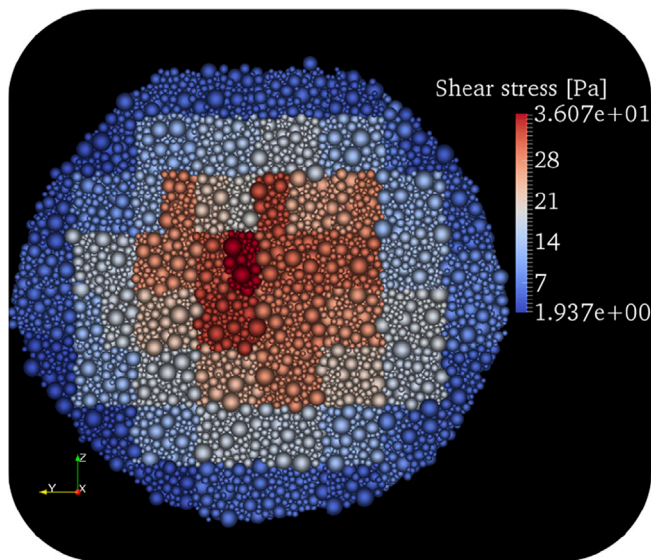


Fig. 11. Shear stress distribution in a stable discrete model of the primary (in cross section). Material friction angle $\sim 38^\circ$, packing efficiency $\sim 75\%$, power-law particle size distribution. The blocky pattern shows elements used for the calculations.

7.3. Binary system internal dynamics

The Didymos binary system is an example of the full two-body problem, characterized by fully coupled rotational and translational dynamics. Detailed simulation of these dynamics has been performed as part of an independent verification and validation effort. In this, two independent software implementations of the same formulation for both force model and numerical integrator were created by personnel at JPL and at GSFC. The force model used was the polyhedral mutual gravity potential formulation (Fahnestock and Scheeres, 2006), while a low-order fixed-step variational integrator, specially suited for preserving geometrical properties and also symplectic, was used (Lee et al., 2007; Fahnestock and Scheeres, 2008).

The shape model illustrated in Fig. 9 (having 1996 facets) was used for the primary, while a purely notional shape model (296 facets) was stretched/scaled on each axis to match the nominal ellipsoid axial ratios assumed in the mission's current Didymos Reference Model (DRM). With adoption of nominal values from Table 6, we chose values for initial misalignment between the primary spin pole and mutual orbit pole, for initial mutual orbit eccentricity, for initial secondary libration angle, and for initial deviation in secondary angular velocity from the synchronous angular velocity (so as to relax most libration amplitudes) all consistent with the DRM within its uncertainties.

For cases matching the earlier-stated (fully relaxed) assumption of zero pole misalignment, and with a plausible very small initial mutual orbit eccentricity of 0.01, and zero initial libration angle, we observed stable motions for ~ 4000 orbits. This number corresponds to our maximum simulation durations (limited by computational resources), not a loss of stability. Variations in mutual orbit semi-major axis, eccentricity, and inclination were ~ 1 m, < 0.015 , and < 0.07 deg, respectively, for simulation duration. Variation in primary spin axis obliquity was < 0.01 deg. The libration amplitude, with our tweaking of secondary angular velocity to mostly eliminate free libration, remained between 1.5 and 2 deg. Assuming a tidally evolved system, the equilibrium state in which the system likely lies is characterized by a small forced eccentricity of ~ 0.005 – 0.010 (depending on actual secondary axial ratios) and a minimum forced libration amplitude of ~ 1 – 2 deg.

A DART impact capable of changing the orbital period of the secondary by ~ 200 s would also induce an eccentricity change of ~ 0.010 – 0.015 . Depending on impact geometry and secondary axial

ratios, such an impact could excite the target's libration by as much as ~ 10 deg, which may or may not be observable from Earth, depending on the secondary rotational light curve amplitude and accuracy of photometric measurements (Pravec et al., 2016). The excitation of libration and eccentricity will be measurable by the Hera rendezvous spacecraft (Michel et al., 2017).

7.4. Dynamical perturbations

The DART impact is expected to change the orbital period of the Didymos secondary by ~ 7 min (Cheng et al., 2016). It is necessary to understand any natural perturbative effects that may mask the impact signal. The Sun will contribute the largest tidal effect on the system, but at a level > 10 times below that anticipated for the impact itself. Due to the eccentric heliocentric orbit, variations in the binary period of up to 17 s will occur over the course of the heliocentric orbit. A careful understanding of the phase of the system at impact will be needed to reduce uncertainties of the impact effect on libration and orbital period. Formally, Earth tides can be slightly stronger than solar tides, but the necessary orbital configuration will not occur before or during encounter.

Thermal re-radiation from the Didymos secondary will lead to the binary-YORP (BYORP) effect (Čuk and Burns, 2005), which can cause a long-term secular change to the binary semimajor axis. Without a detailed shape model of the secondary, its estimated ellipsoid shape can be used, along with density and orbit properties from Table 6, to scale the BYORP rate from 1999 KW4 (McMahon and Scheeres, 2010). This shows that if the deviation in the shape of the Didymos secondary from a perfect ellipsoid is similar to that of the 1999 KW4 secondary, the Didymos orbit semimajor axis may grow/shrink at ± 1.66 cm yr $^{-1}$. This translates to a mean quadratic anomaly drift rate of $\pm 2.8^\circ$ yr $^{-2}$, or a very small period drift of 0.91 s yr $^{-1}$. If the BYORP effect is working to shrink the binary orbit, intercomponent tidal forces can oppose the effect, resulting in a constant orbit size (Jacobson and Scheeres, 2011), as is hypothesized for 1996 FG3 (Scheirich et al., 2015; McMahon et al., 2016).

7.5. Other dynamical effects

Given the fast rotation and nominal physical parameters of the primary, centrifugal force may overcome gravitational force at low latitudes, allowing regolith material of any size to go through take-off/landing cycles and cause loss of fines due to solar radiation pressure. Analysis of this effect accounting for the current shape model is ongoing to estimate the effective mass density of floating material in the neighborhood of the primary. These considerations apply equally well to the secondary, with the added complication that escaping material can remain bound to the primary.

The DART impact will eject particles with a wide velocity distribution relative to the secondary surface, as predicted by various point-source crater scaling laws or higher-fidelity impact simulations. Given the near-critical state of the primary, if high-speed ejecta from the secondary hit the primary, this may disturb the primary's structure. Consider an ejecta cone with angle 45° from the surface normal at various locations on the secondary, and assumed ballistic flight of particles (> 10 m/s) subject to no forces. If the impact site deviates 30 m from the currently planned location, fast ejecta from the secondary will hit the surface of the primary. This might trigger landslides that would alter the shape, material distribution, and therefore the gravity field of the primary (Hirabayashi et al., 2017), while perhaps providing an opportunity to better understand granular physics in microgravity. If there is a significant shape change of the primary after the impact, there will be a corresponding change in rotation period which will be measured by ground-based observations.

8. Conclusions

The AIDA mission will combine US and European space experience

and expertise to address an international concern, the asteroid impact hazard. AIDA will perform the first demonstration of asteroid deflection by a kinetic impactor. The target of the AIDA mission will be the binary asteroid (65803) Didymos, in which DART will target the secondary, smaller member in order to alter its orbit around the primary. The resulting period change will be measured by Earth-based observations. The asteroid deflection will be measured to higher accuracy, and additional results of the DART impact, like the impact crater, will be studied in great detail by the Hera mission. AIDA will return vital data to determine the momentum transfer efficiency of the kinetic impact and key physical properties of the target asteroid. The two mission components of AIDA, DART and Hera, are each independently valuable, but when combined they provide a greatly increased knowledge return for planetary defense and planetary science. They are also associated with challenges that can capture the interest of the public and young generations.

Acknowledgements

The AIDA DART studies were supported by NASA at JHU/APL under Contract # NNN06AA01C, Task Order # NNN15AA05T, and the AIM and Hera studies were funded by ESA. We thank the science and engineering teams at APL for enthusiastic and dedicated support. The work of PP was supported by the Grant Agency of the Czech Republic, Grant 17-00774S.

References

- Barnouin-Jha, O.S., Cheng, A.F., Mukai, T., Abe, S., Hirata, N., Nakamura, R., Gaskell, R.W., Saito, J., Clark, B.E., 2008. Small-scale topography of 25143 Itokawa from the Hayabusa laser altimeter. *Icarus* 198, 108–124.
- Benner, L.A.M., et al., 2010. Radar imaging and a physical model of binary asteroid 65803 Didymos. *DPS* 42, 1317 (abstract).
- Campo Bagatin, A., Aleman, R.A., Benavidez, P.G., Richardson, D.C., 2018. Internal structure of asteroid gravitational aggregates. *Icarus* 302, 343–359.
- Carnelli, I., Galvez, A., Ongaro, F., 2006. Learning to deflect near-Earth objects: industrial design of the Don Quijote mission. In: 57th International Astronautical Congress, Valencia, Spain. <https://doi.org/10.2514/6.IAC-06-A3.5.05>.
- Cheng, A.F., et al., 2008. Long-range reconnaissance imager on New Horizons. *Space Sci. Rev.* 140, 189. <https://doi.org/10.1007/s11214-007-9271-6>.
- Cheng, A.F., et al., 2015. Asteroid impact and deflection assessment mission. *Acta Astronaut.* 115, 262–269. <https://doi.org/10.1016/j.actaastro.2015.05.02>.
- Cheng, A.F., et al., 2009. Fundamentally distinct outcomes of asteroid collisional evolution and catastrophic disruption. *Planet. Space Sci.* 57, 165–172.
- Cheng, A.F., et al., 2016. Asteroid Impact & deflection assessment mission: kinetic impactor. *Planet. Space Sci.* 121, 27–35.
- Čuk, M., Burns, J.A., 2005. Effects of thermal radiation on the dynamics of binary NEAs. *Icarus* 176, 418–431.
- De Leon, J., Licandro, J., Serra-Ricart, M., Pinilla-Alonso, N., Campins, H., 2010. Observations compositional, and physical characterization of near-Earth and Mars-crosser asteroids from a spectroscopic survey. *A&A* 517, A23. <https://doi.org/10.1051/0004-6361/200913852>.
- DeMeo, F., Binzel, R.P., Lockhart, M., 2014. Mars encounters cause fresh surfaces on some near-Earth asteroids. *Icarus* 227, 112–122.
- Dunn, T.L., Burbine, T.H., Bottke, W., Clark, J.P., 2013. Mineralogies and source regions of near-Earth asteroids. *Icarus* 222, 273–282.
- Fahnstocck, E.G., Scheeres, D.J., 2006. Simulation of the full two rigid body problem using polyhedral mutual potential and potential derivatives approach. *Celestial Mech. Dyn. Astron.* 96, 317–339.
- Fahnstocck, E.G., Scheeres, D.J., 2008. Simulation and analysis of the dynamics of binary near-Earth asteroid (66391) 1999 KW4. *Icarus* 194, 410–435.
- Fujiwara, A., et al., 2006. The rubble-pile asteroid itokawa as observed by hayabusa. *Science* 312, 1330–1334.
- Gaskell, R.W., et al., 2008. Characterizing and navigating small bodies with imaging data. *Meteorit. Planet. Sci.* 43, 1049–1061.
- Grieger, B., Kueppers, M., 2016. Determining the mass of Didymos' secondary by visual imaging. *EGU General Ass. Conf. Abs.* 18, EPSC2016.
- Harris, A.W., D'Abramo, G., 2015. The population of Near-Earth asteroids. *Icarus* 257, 302–312.
- Herique, A., Agnus, B., Asphaug, E., et al., 2017. Direct observations of asteroid interior and regolith structure: science measurement requirements. *Adv. Space Res.* <https://doi.org/10.1016/j.asr.2017.10.020>.
- Hirabayashi, M., Scheeres, D.J., 2016. Failure mode diagram of rubble pile asteroids. *Proc. IAU Symp.* 318, 122–127.
- Hirabayashi, M., et al., 2017. Constraints on the perturbed mutual motion in Didymos due to impact-induced deformation of its primary after the DART impact. *Mon. Not. Roy. Astron. Soc.* 472, 1641–1648.
- Holsapple, K.A., Housen, K.R., 2007. A crater and its ejecta: an interpretation of Deep Impact. *Icarus* 187, 345–356.
- Holsapple, K.A., Housen, K.R., 2012. Momentum transfer in asteroid impacts. I. theory and scaling. *Icarus* 221, 875–887.
- Jacobson, S.A., Scheeres, D.J., 2011. Dynamics of rotationally fissioned asteroids: source of observed small asteroid systems. *Icarus* 214, 161–178.
- Jutzi, M., Michel, P., 2014. Hypervelocity impacts on asteroids and momentum transfer. I. numerical simulations using porous targets. *Icarus* 229, 247–253.
- Kohout, T., et al., 2017. Feasibility of asteroid exploration using CubeSats ASPECT case study. *Adv. Space Res.* <https://doi.org/10.1016/j.asr.2017.07.036>.
- Lee, T., et al., 2007. Lie group variational integrators for the full body problem in orbital mechanics. *Celestial Mech. Dyn. Astron.* 98, 121–144.
- Marshall, J., Rizk, B., 2015. Rounded boulders on Itokawa as clues to geological processes in the early solar system. *Planet. Space Sci.* 119, 181–184.
- Mazrouei, S., Daly, M.G., Barnouin, O.S., Ernst, C.M., DeSouza, I., 2014. Block distributions on Itokawa. *Icarus* 229, 181–189.
- McMahon, J.W., Scheeres, D.J., 2010. Detailed prediction for the BYORP effect on binary near-Earth asteroid (66391) 1999 KW4 and implications for the binary population. *Icarus* 209, 494–509.
- McMahon, J.W., et al., 2016. LPI 47, 2285.
- Michel, P., et al., 2016. Science case for the Asteroid impact Mission (AIM): a component of the Asteroid Impact & Deflection Assessment (AIDA) mission. *Adv. Space Res.* 57, 2529–2547.
- Michel, P., 2013. Physical properties of near-earth objects that inform mitigation. *Acta Astronaut.* 90, 6–13.
- Michel, P., et al., 2017. European component of the AIDA mission to the binary asteroid Didymos: characterization and interpretation of the impact of the DART mission. *Adv. Space Res.* <https://doi.org/10.1016/j.asr.2017.12.020>.
- Michel, P., O'Brien, D.P., Abe, S., Hirata, N., 2009. Itokawa's cratering record as observed by Hayabusa: implications for its age and collisional history. *Icarus* 200, 503–513.
- Michikami, T., et al., 2008. Size-frequency statistics of boulders on global surface of asteroid 25143 Itokawa. *Earth Planets Space* 60, 13–20.
- Michikami, T., Hagermann, A., Kadokawa, T., Yoshida, A., Shimada, A., Hasegawa, S., Tsuchiyama, A., 2016. Fragment shapes in impact experiments ranging from cratering to catastrophic disruption. *Icarus* 264, 316–330.
- Michikami, T., Nakamura, A.M., Hirata, N., 2010. The shape distribution of boulders on Asteroid 25143 Itokawa: comparison with fragments from impact experiments. *Icarus* 207, 277–284.
- Miyamoto, H., et al., 2007. Regolith migration and sorting on asteroid itokawa. *Science* 316, 1011–1014.
- Noguchi, T., et al., 2010. Surface morphological features of boulders on Asteroid 25143 Itokawa. *Icarus* 206, 319–326.
- Noviello, J.L., Ernst, C.M., Barnouin, O.S., Daly, M., 2014. Block distribution on Itokawa: implications for asteroid surface evolution. *Lunar and Planet. Sci. Conf.* 45, 1587.
- Owen, J.M., Bruck Syal, M., Remington, T., Miller, P.L., Richardson, D., Asphaug, E., 2017. Modeling kinetic impactors on a rubble pile asteroid. In: *IAA Planetary Defense Conference. IAA-PDC-17-04-08*, Tokyo, Japan (abstract).
- Pierazzo, E., et al., 2008. Validation of numerical codes for impact and explosion cratering: impacts on strengthless and metal targets. *Meteorit. Planet. Sci.* 43 (12), 1917–1938.
- Polishook, D., Brosch, N., Priyalnik, D., 2011. Rotation periods of binary asteroids with large separations – confronting the escaping ejecta binaries model with observations. *Icarus* 212, 167–174.
- Pravec, P., et al., 2006. Photometric survey of binary near-Earth asteroids. *Icarus* 181, 63–93.
- Pravec, P., et al., 2016. Binary asteroid population. 3. secondary rotations and elongations. *Icarus* 267, 267–295.
- Rainey, E.S.G., Stickle, A.M., Rivkin, A.S., Barnouin, O.S., Ernst, C.M., Cheng, A.F., 2017. Modeling potential outcomes of the DART impact using CTH. In: *IAA Planetary Defense Conference, IAA-PDC-04-P10*. Tokyo, Japan (abstract).
- Saiki, T., et al., 2017. The Small Carry-on Impactor (SCI) and the Hayabusa-2 impact experiment. *Space Sci. Rev.* 208, 165–186.
- Saito, J., et al., 2006. Detailed images of asteroid 25143 Itokawa from Hayabusa. *Science* 312, 1341–1344.
- Scheeres, D.J., et al., 2016. The geophysical environment of Bennu. *Icarus* 276, 116–140.
- Scheirich, P., Pravec, P., 2009. Modeling of light curves of binary asteroids. *Icarus* 200, 531–547.
- Scheirich, P., et al., 2015. The binary near-Earth asteroid (175706) 1996FG3–An observational constraint on its orbital evolution. *Icarus* 245, 56–63.
- Schwartz, S.R., Richardson, D.C., Michel, P., 2012. An implementation of the soft sphere discrete element method in a high performance gravity tree code. *Gran. Matt.* 14, 363–380.
- Sierks, H., Keller, H.U., Jaumann, R., et al., 2011a. The dawn framing camera. *Space Sci. Rev.* 164, 263–327. <https://doi.org/10.1007/s11214-011-9745-4>.
- Sierks, H., Lamy, P., Barbieri, C., et al., 2011b. Images of asteroid 21 Lutetia: a remnant planetesimal from the early solar system. *Science* 334, 487–490.
- Stickle, A.M., Rainey, E.S.G., Bruck Syal, M., Owen, J.M., Miller, P., Barnouin, O.S., Ernst, C.M., AIDA Impact Simulation Working Group, 2017. Modeling impact outcomes for the Double Asteroid Redirection Test (DART) mission. *Procedia. Eng.* 204, 116–123.
- Stickle, A.M., Atchison, J.A., Barnouin, O.S., Cheng, A.F., Crawford, D.A., Ernst, C.M., Fletcher, Z., Rivkin, A.S., 2015. Modeling momentum transfer from kinetic impacts: implications for redirecting asteroids. *Proced. Eng.* 103, 577–584. <https://doi.org/10.1016/j.proeng.2015.04.075>.
- Stickle, A.M., et al., 2016. Impact Simulation Benchmarking for the Double Asteroid Redirect Test (DART). *LPSC, The Woodlands, TX. Abstract #2832*.
- Syal, M.B., Owen, J.M., Miller, P.L., 2016. Deflection by kinetic impact: Sensitivity to asteroid properties. *Icarus* 269, 50–61.

- Tancredi, G., Roland, S., Bruzzone, S., 2015. Distribution of boulders and the gravity potential on asteroid Itokawa. *Icarus* 247, 279–290.
- US National Research Council Committee to review Near-Earth Object Surveys and Hazard Mitigation Strategies, 2010. *Defending Planet Earth: Near-Earth Object Surveys and Hazard Mitigation Strategies*. <http://www.nap.edu/catalog/12842.html>.
- Viikinkoski, M., Kaasalainen, M., Āurech, J., 2015. ADAM: a general method for using various data types in asteroid reconstruction. *Astron. Astrophys.* 576, A8–A11.
- Walsh, K.J., Richardson, D.C., Michel, P., 2008. Rotational breakup as the origin of small binary asteroids. *Nature* 454, 188–191.
- Weaver, H.A., et al., 2016. The small satellites of Pluto as observed by New Horizons. *Science* 351 aae0030–aae0030.
- Zannoni, M., et al., 2017. Radio science investigations with the asteroid impact mission. *Adv. Space Res.* <https://doi.org/10.1016/j.asr.2017.12.003>.
- Zhang, Y., Richardson, D.C., et al., 2017. Creep stability of the proposed AIDA mission target 65803 Didymos: I. discrete cohesionless granular physics model. *Icarus* 294, 98–123.